The switching between zonal and blocked mid-latitude atmospheric circulation: a dynamical system perspective

Davide Faranda, Giacomo Masato, Nicholas Moloney, Yuzuru Sato, François Daviaud, Bérengère Dubrulle, Pascal Yiou

A dynamical mechanism for the switching between zonal and blocked mid-latitude atmospheric circulation.

Davide Faranda*

LSCE, CEA Saclay l'Orme des Merisiers,

CNRS UMR 8212 CEA-CNRS-UVSQ, 91191 Gif-sur-Yvette, France

Giacomo Masato

Department of Meteorology/NCAS, University of Reading, Reading, UK

Nicholas R. Moloney

London Mathematical Laboratory, 14 Buckingham Street, London WC2N 6DF, UK

Yuzuru Sato

RIES/Department of Mathematics, Hokkaido University,

Kita-ku, Sapporo, Hokkaido 060-0812, Japan

Francois Daviaud and Bérengère Dubrulle

Laboratoire SPHYNX, SPEC, CEA Saclay,

CNRS UMR 3680, 91191 Gif-sur-Yvette, France

Pascal Yiou

LSCE, CEA-Saclay l'Orme des Merisiers,

CNRS UMR 8212 CEA-CNRS-UVSQ, 91191 Gif-sur-Yvette, France

Abstract

Atmospheric mid-latitude circulation is dominated by a zonal, westerly flow. Such a flow is generally symmetric, but it can be occasionally broken up by blocking anticyclones. The subsequent asymmetric flow can persist for several days. In this paper, we apply new mathematical tools in order to reexamine the dynamical mechanisms responsible for the transitions between zonal and blocked flows. By analyzing several blocking indices, we discard the general claim that mid-latitude circulation features two distinct stable equilibria or chaotic regimes, in favor of a simpler mechanism that is well understood in dynamical systems theory: we identify the blocked flow as an unstable fixed point (or saddle point) of a single basin chaotic attractor, dominated by the westerlies regime. We also analyze the North Atlantic Oscillation and the Arctic Oscillation atmospheric indices, whose behavior is often associated with the transition between the two circulation regimes, and investigate analogies and differences with the bidimensional blocking indices. We find that the Arctic Oscillation index, which is a proxy for a global average of the Tibaldi-Molteni blocking index, keeps track of the presence of unstable fixed points. On the other hand, the North Atlantic Oscillation index is representative only of local properties of the North Atlantic blocking dynamics.

*Electronic address: davide.faranda@cea.fr

I. INTRODUCTION

In the time range of 2 – 8 days, the mid-latitude large scale circulation is driven by the destabilization of a westerly sheared jet, associated with a meridional temperature gradient [1]. The destabilizing mechanism is referred to as the baroclinic instability and it consists in the appearance of three dimensional wave structures (extra-tropical cyclones and anticyclones) normally embedded in the mid-latitude westerlies. The minimal model for such an instability is known as the Charney-Eady model [2]. Such a model is based on the stability analysis of the quasi-geostrophic potential vorticity equation coupled with a thermodynamic equation. The stability parameter is the Burger number, i.e. the ratio between stratification (a quantity linked to the meridional temperature gradient) and rotational effects. The Charney-Eady model explains most of the energy transfer between the potential energy in the atmosphere's pole-to-equator temperature difference and the kinetic energy of cyclones.

Cyclones and anticyclones are generally embedded in the mid-latitude jet, and have average lifetimes of a few days that depend on their size, longitudinal asymmetry and interaction with the topography [3, 4]. However, a few times per year and with higher frequency in the winter season, large high-pressure structures may form and persist for several days, breaking up the westerlies circulation and forcing the jet to move towards higher latitudes or even split up into two branches, hence breaking the longitudinal symmetry. This kind of circulation is referred to as blocked flow and it has produced a few extreme climate events like the December 2010 cold spell in northern and central Europe, the warm winter of 2006/2007 [5] or the persistence of Arctic low pressure (Summer 2002) with a remarkable negative record of arctic sea ice extent [6]. It is therefore crucial to get a complete understanding of the blocked flow and of the mechanism which regulates the transition to the westerlies regime.

In order to understand the transition mechanism among these flow regimes, many studies of mid-latitude dynamics have been conducted both theoretically and experimentally. Legras and Ghil [7, 8] have shown the intricacy of such circulation by studying an intermediate complexity model of a barotropic flow with dissipation forcing and topography. The

authors observed two distinct equilibria which can be associated with either the westerlies or the blocked flows. Similar conclusions appear in [9] and are supported by experimental laboratory studies [10]. More recent works question such a theoretical framework on the basis of observations [11–13]: blocking appears as a distinctive dynamical feature with respect to westerlies circulation, but it consists of several multistable patterns.

In this paper we reanalyse data over the past decades to detect whether the dynamics of blocking is compatible with the existence of an unstable fixed point of the atmospheric mid-latitude circulation. This evidence comes from dynamical systems theory and is supported by the common experience that, within the blocked flow, atmospheric variables follow a highly predictable dynamics (persistence of the same weather conditions for several days), whereas in the zonal flow they mostly have a chaotic behavior (irregular alternation between cyclonic and anticyclonic phases). Such kind of dynamical features are also encountered for several dynamical systems systems ranging from toy models (Pomeau-Manneville map, Hénon map, Lorenz equations [14]) to intermediate complexity models [15, 16]. The dynamics of all these systems is generally chaotic and takes place on a single basin chaotic attractor, but is sometimes trapped near an unstable fixed point. When this happens, an orbit stays in the vicinity of the fixed point for an amount of time which depends on the distance from the point and its dynamical properties. As a result, the system experiences a local suppression of chaos.

We propose to detect the existence of unstable fixed points in the mid-latitude atmospheric circulations by using recent results obtained for recurrences of dynamical systems [17–20]. These results have opened a new branch of research where recurrences of a certain observation in an orbit are treated via the statistics of extreme events. The novelty of this approach lies in the fact that classical extreme value laws can be found for such recurrences for almost every point of chaotic attractors [17]. In [21] we have exploited this technique to study instrumental temperature records, verifying that temperature recurrences obey ones of the three classical extreme values, i.e. the atmosphere behaves as a chaotic system. Via this analysis, a map can be constructed of European temperatures whose recurrence is likely or unlikely with respect to a certain time scale of interest.

In order to detect the possible unstable fixed points of the atmospheric dynamics, we will analyze several blocking indices. In general, a blocking index is defined in terms of the difference of pressure (or conjugated fields) between two different locations at the same longitude. When the flow is zonal, this difference always has the same sign because anticyclones are generally located at lower latitudes. Conversely, when the flow is blocked, low pressure systems tend to move to low latitudes and anticyclones to high latitudes, reversing the meridional gradient in pressure. A blocking event is identified as the persistence of such conditions for several days.

We will begin our analysis with the Tibaldi-Molteni index [22], defined at each longitude via differences of geopotential heights, and compare the results with those obtained for the bidimensional blocking index introduced by Pelly et al [23], where differences are taken over a potential vorticity surface closer to the tropopause and to the core of the jet stream. After collecting evidence for the existence of unstable fixed points and their spatial distribution, we will perform the analysis on one-dimensional indices of atmospheric circulation to see whether they keep any trace of the existence of unstable fixed points. In particular, we will focus on the Artic Oscillation (AO) index, which is roughly a global average of the Tibaldi-Molteni index, and on the North Atlantic Oscillation (NAO) index, defined as the difference between the pressure in Lisbon and Reykjavik — and therefore representative of the North-Atlantic/European regions only.

The paper is organized as follows: in section 2, we give an overview of the method and explain the analogy between unstable fixed points and blocked circulation via dynamical systems toy models. In section 3, we present evidence for the existence of unstable fixed points by using the Tibaldi-Molteni and the Pelly blocking indices. In section 4, we analyze the role of one-dimensional indices, such as the AO and the NAO. The analysis will show that, although the one-dimensional indices are used to highlight features of the mid-latitude circulation, the local nature of the NAO makes it inadequate for global properties. Finally, we discuss how to improve the modeling of the mid-latitudes circulation on the basis of the results obtained.

II. METHOD AND RESULTS FROM DYNAMICAL SYSTEMS

In this section we A) show how to detect unstable fixed points in dynamical systems and time series, B) explain the inference procedures, and C) discuss the estimation of the parameters describing the statistical properties of the unstable point.

A. Detection of unstable fixed points via dynamical systems techniques

Let us consider a discrete-time dynamical system. This is a relevant hypothesis for an atmospheric system [24], as both models and observations are made at discrete times. The dynamics is governed by the map T, which iterates the variables of the system x according to

$$x_{t+1} = T(x_t). \tag{1}$$

We assume that, by starting from a random initial condition, the dynamics follows a chaotic trajectory on a well-defined surface of the phase space, i.e. the attractor. We fix a point ζ on the attractor and measure the time series of the distances between ζ and the subsequent iterations of the orbit:

$$w(t;\zeta) = -\log(d(T(x_t),\zeta)),$$

where d is a distance function between two vectors. We are interested in the high extremes of $w(t;\zeta)$, for all t. By construction, such extremes define the recurrences of the system. To identify the extremes, we apply the block-maxima approach. It consists of dividing the time series $T(x_t)$ into intervals of length m. Every m observations, the closest recurrence to the point ζ is taken. If n intervals of length m are available in the series, one obtains n closest recurrences. If the system is chaotic, the logarithmic weight forces the asymptotic extreme value distribution to follow a Gumbel law. A detailed explanation for this can be found in [21], but the reason is intuitive: the Gumbel law is of the form $G(x) = \exp(-\exp(-x))$. One of the exponential functions comes from the exponential recurrence statistics, the other from the inverse of the logarithm. Other choices for w, typically power laws, constrain the asymptotic extreme distribution to be either a Weibull or a Fréchet.

This theoretical framework applies to almost all the points of a chaotic attractor except at the unstable fixed points. A fixed point of the system in Eq. (1) is one that repeats itself under iteration, i.e. $T(x) = x$. An unstable or repelling fixed point is one for which the distance between itself and any point in a surrounding neighborhood increases under iterations [25]. A theoretical result from dynamical systems, obtained by [19], states that when ζ is an unstable fixed point of the recurrence map T, then the distribution of $w(t;\zeta)$ follows a modified Gumbel law:

$$G(x,\theta) = \exp(-\exp(-\theta x)),$$

where θ is a parameter known as the extremal index.
The concept of the extremal index appears in classical extreme value theory, where θ gives a measure of 'clustering', i.e. the tendency of random variables to exceed a threshold consecutively. If a threshold u is applied to a series of observations $x_1, x_2, \ldots, x_s$, the exceedances are those for which $x_i > u$. Heuristically, the extremal index can then be thought of as $\theta = 1/\ell$, where ℓ is the mean duration of consecutive exceedances (clusters), i.e. the average of the time intervals spent above u.

The extremal index also finds useful application in dynamical systems [19], where θ can vary across the phase space according to the chosen ζ from which recurrences are measured. Clustering occurs when consecutive iterates of the orbit are observed near a point of the attractor. For almost all the nonsingular points there is no clustering. This means that, on average, an orbit enters the neighborhood of ζ once at time, which gives $\theta = 1$. However, when ζ is close to an unstable fixed point, $\theta < 1$. The smaller the θ, the larger the cluster size, i.e. the longer the time the orbit stays in the vicinity of ζ. In the dynamical systems context, the cluster extends in both time and space: we observe a time cluster in the minimum distances between the unstable fixed point and the orbit. This in turn effectively corresponds to a spatial cluster because the orbits are held within the vicinity of the unstable fixed point.

As an example, we consider the Hénon attractor [26] shown in Fig.1–a), obtained by iterating

the following set of equations:

$$\begin{aligned} x_{t+1} &= y_t + 1 - 1.4x_t^2, \\ y_{t+1} &= 0.3x_t. \end{aligned} \tag{2}$$

In this picture, the presence of the unstable fixed point ζ_u is not obvious. Its existence can be proved analytically by solving $T(x, y) = (x, y)$, with approximate solution $\zeta_u = (0.63, 0.19)$, as indicated in Fig.1-a). The dynamics around this point is different from that of a generic point, and this can be captured by computing the recurrences. Figs.1b and .1c show distances of iterates of the orbit measured from ζ_u and a generic point ζ of the attractor, respectively. In the former case, a long cluster is clearly visible and its length can be determined via the extremal index θ or by using the formula given in [19].

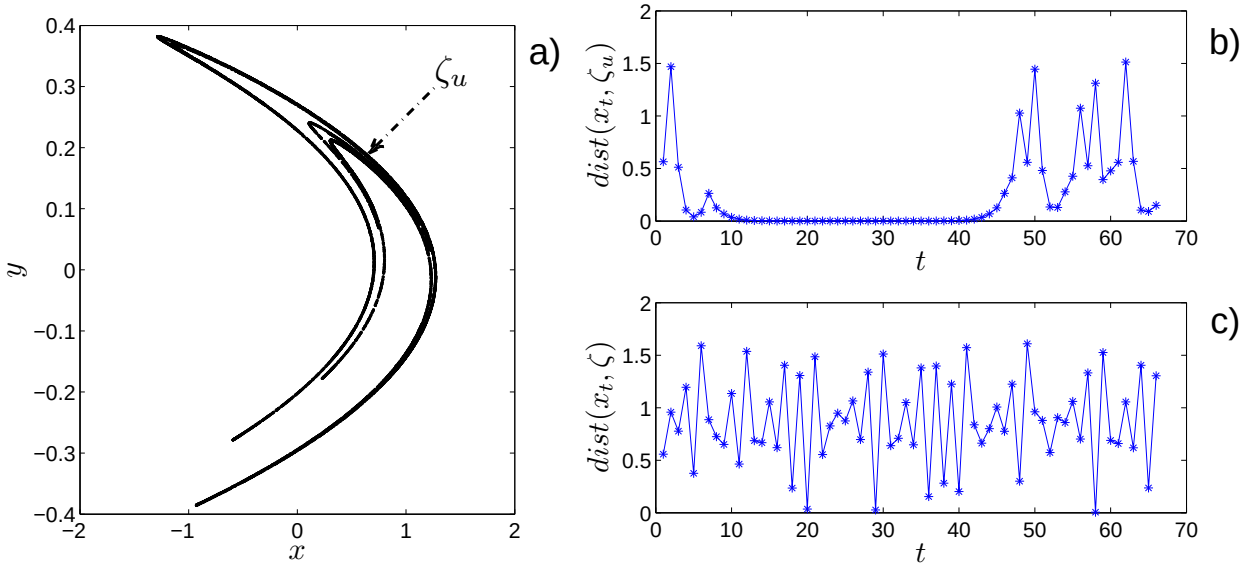

FIG. 1: a) Hénon attractor, obtained by iterating Eq. (2). The location of the unstable fixed point ζ_u is indicated. b) Series of distances from the unstable fixed point ζ_u. Clustering occurs when the trajectory gets close to ζ_u. c) Series of distances from a generic point of the attractor ζ. No clustering occurs.

Although the Hénon dynamics is not representative of the atmospheric circulation, it is helpful to illustrate the general dynamical behavior around an unstable fixed point. In chaotic dynamical systems we can only observe clustering at unstable fixed points (see [19] , Theorem 1), independently of the complexity of the system. If we consider the time series of

observations as the output of a dynamical system, then we may hope to track the presence of unstable fixed points by measuring $\theta < 1$ for some reference values ζ.

B. Algorithm and inference of the extremal index

In order to compute the extremal index θ for time series we will use the following algorithmic procedure:

1. Consider a time series consisting of s observations: $\{x(t) : t = 1, 2, ..., s\}$.
2. Fix ζ to be a point of the series itself.
3. Compute the series $w(t; \zeta) = -\log(d(x(t), \zeta))$.
4. Take a very high quantile q of the $w(t)$ distribution, in order to consider only the closest recurrences (when $d(x, \zeta)$ is small, $w(x, \zeta)$ is large).
5. Compute the extremal index.

While θ can be thought of as the inverse mean cluster size, a more robust estimator of the extremal index is that constructed by Süveges [27], which, for a fixed quantile q, reads:

$$\theta = \frac{\sum_i (1-q)S_i + N + N_c - \sqrt{\left(\sum_i^{N_c}(1-q)S_i + N + N_c\right)^2 - 8Nc\sum_i^{N_c}(1-q)S_i}}{2\sum_i (1-q)S_i},$$

where N is the number of $w(t, \zeta)$ above the chosen quantile, N_c the number of observations which form a cluster of at least two consecutive recurrences, and S_i the length of each cluster i.

C. Finite-size effects

In [28] we have discussed some of the problems related to the finiteness of datasets when studying the recurrences around a certain value in a time series. The results $\theta = 1$ at generic points and $\theta < 1$ at unstable fixed points hold only in the limit $q \to 1$. When dealing with finite data sets, the limit $q \to 1$ is unattainable and, depending on the marginal distribution, some points ζ may be associated with an extremal index $\theta < 1$

even when they are not unstable fixed points. To illustrate this effect, we analyse a time series generated by an auto-regressive process of order 1, $x(t) = \phi x(t-1) + \epsilon(t)$, where $|\phi| < 1$ is the magnitude of the auto-regressive coefficient and $\epsilon(t)$ is a random variable drawn from a normal distribution. It is theoretically known that the extremes of this process do not cluster in the limit $q \to 1$, so that $\theta = 1$ for all ζ and all ϕ. However, for finite datasets and fixed q, clustering will be observed among the weakly (exponentially) correlated exceedances all the while they have not exited from a window around ζ whose size is a function of ϕ and the underlying marginal density. For larger ϕ and ζ chosen in the wings of the marginal density, the greater the 'finite-size' clustering. In our numerical experiment, we take $\phi = 0.5$ and synthetic datasets of lengths 30000 (of the order of the real time series we later analyse) and 300000. In Fig. 2 we plot the empirical marginal densities in the left panel, and the computed θ as a function of ζ in the central panel. Note that $\theta < 1$ in the wings of the distribution, even though the model has no inherent tendency to cluster extremes.

Our method to deal with such finite-size effects is based on the following observations: the extremal index obtained for some fixed $q < 1$ depends on i) the shape of the marginal density, ii) the spectral properties of the process (i.e. ϕ in our above example), iii) the choice of ζ, since clustering is a *local* property.

We have tested i) and ii) by changing both the marginal and the magnitude of the coefficient ϕ, which is directly linked to the spectrum for the process[29]. We can go further by generating surrogates of the original dataset that have identical marginal distributions and, to within a very low tolerance, the same spectral properties. In this way we can 'subtract' the effects of i) and ii) in the computation of θ. To perform this in practice, we use the Iterative Amplitude Adjusted Fourier Transform (IAAFT) of Schreiber and Schmitz [30]. In order to compute the residual extremal indices, which we will denote by $\theta^*(\zeta)$, it is sufficient to average over several surrogate estimates of θ, such that:

$$\theta^*(\zeta) = \langle \theta(\zeta, x_{\mathrm{SURR}}) \rangle - \theta(\zeta, x), \tag{3}$$

where the $\langle\rangle$ are averages over realizations of surrogate data. This procedure has been tested on the auto-regressive samples previously analysed. The residual θ^* is plotted in the right

panel of Fig. 2. As expected from theory, there is no local clustering.

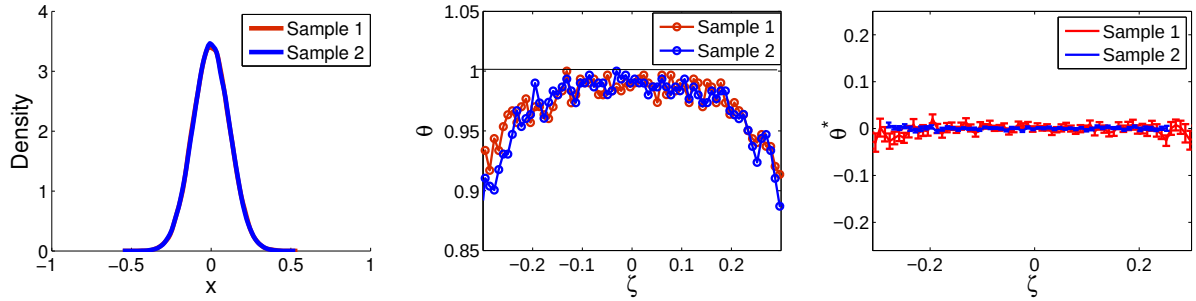

FIG. 2: Left panel: empirical density for data generated by an autoregressive process. Central panel: extremal indices θ computed at 100 reference points ζ. Right panel: residual extremal index θ^* computed at the same ζ as in the central panel. Sample 1 contains 30000 data. Sample 2 contains 300000 data.

An analysis of the Hénon attractor provides a test of property iii). Here, we can check whether we are able to recover the known location of the unstable fixed point via a computation of θ^* for the time series of x and y. Results are shown in Figure 3 for 30000 observations. The location of ζ_u is picked out by the two peaks of θ^* at $x = 0.63$ (left panel) and $y = 0.19$ (right panel). Secondary peaks are also visible in these plots, which are related to the influence of ζ_u in nearby locations of the attractor.

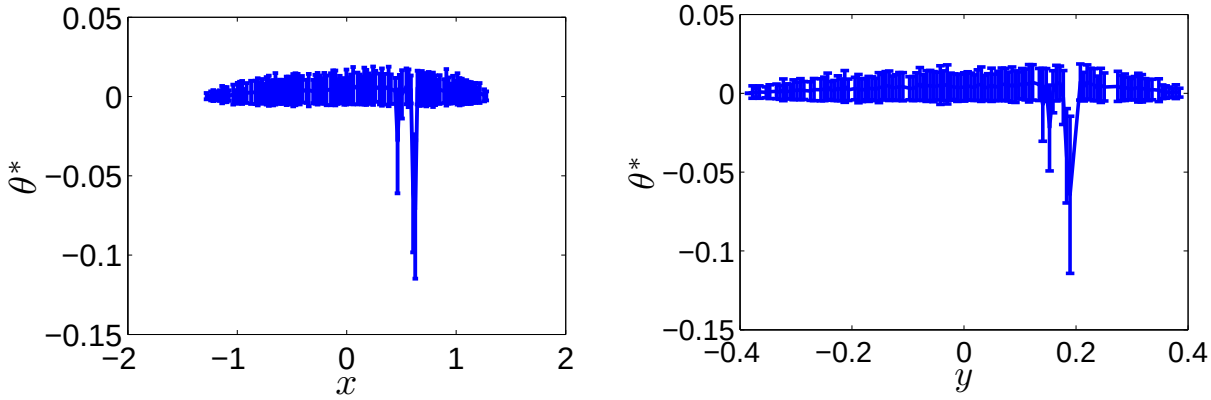

FIG. 3: Residual extremal index θ^*, based on 30000 iterations of the Hénon map. Left panel: x observable. Right panel: y observable.

III. ANALYSIS OF MULTIDIMENSIONAL BLOCKING INDICES

In the following analysis we generate 100 surrogates to compute $\langle\theta(\zeta, x_{\mathrm{SURR}})\rangle$, and take $q = 0.995$. We find that our results are robust with respect to quantile provided $q \gtrsim 0.99$. The first bidimensional blocking index was introduced by Scherrer et al. [31] and it is based on the original definition given by Tibaldi and Molteni [22, 32]. This index determines the longitudinal asymmetry of the atmospheric flow between 40°N and 80°N, by comparing meridional gradients of geopotential height at 500hPa (Z). For each longitude in the northern extra-tropics, a southern gradient B_S and a northern gradient B_N of Z are computed as follows:

$$B_S = \frac{Z(\phi_o) - Z(\phi_S)}{\phi_o - \phi_s}$$

$$B_N = \frac{Z(\phi_n) - Z(\phi_0)}{\phi_n - \phi_s}$$

where $\phi_n = 80° + \delta$, $\phi_0 = 60° + \delta$, $\phi_s = 40° + \delta$, $\delta = -5°, 0°, 5°$. A given longitude is considered to be *blocked* at a given time if the following two conditions are satisfied for at least one value of δ:

$$(1):\ B_S > 0, \qquad (2):\ B_N < -10 \text{ m/degree}$$

Here, we analyze daily time series of $B_S(t)$ computed for the Z field of the National Centers for Environmental Prediction (NCEP) daily reanalysis [Kalnay et al., BAMS, 1996], which represent the strength of the Tibaldi-Molteni blocking index, under the condition that $B_S > 0$ and $B_N < -10$. Blocking events mainly occur around 180° (in the Pacific) and at 0° (in the Eastern North Atlantic) longitude [33]. For our analysis, positive values of $B_S(t)$ also satisfying condition (2) are considered. The values of θ^* plotted in Figure 4 are computed using the technique described in the previous section, with 100 reference points of $\zeta = B_S$. Some areas attain remarkably negative values of θ^* and, over all, the average extremal index is negative at all longitudes (lower panel of Figure 4). Therefore, for these areas the dynamics of blocking is compatible with the existence of unstable fixed points. It is quite surprising to observe that at 0° longitude θ^* is close to zero, implying no clustering. Although the European region is affected by strong blocking events, the clustering of B

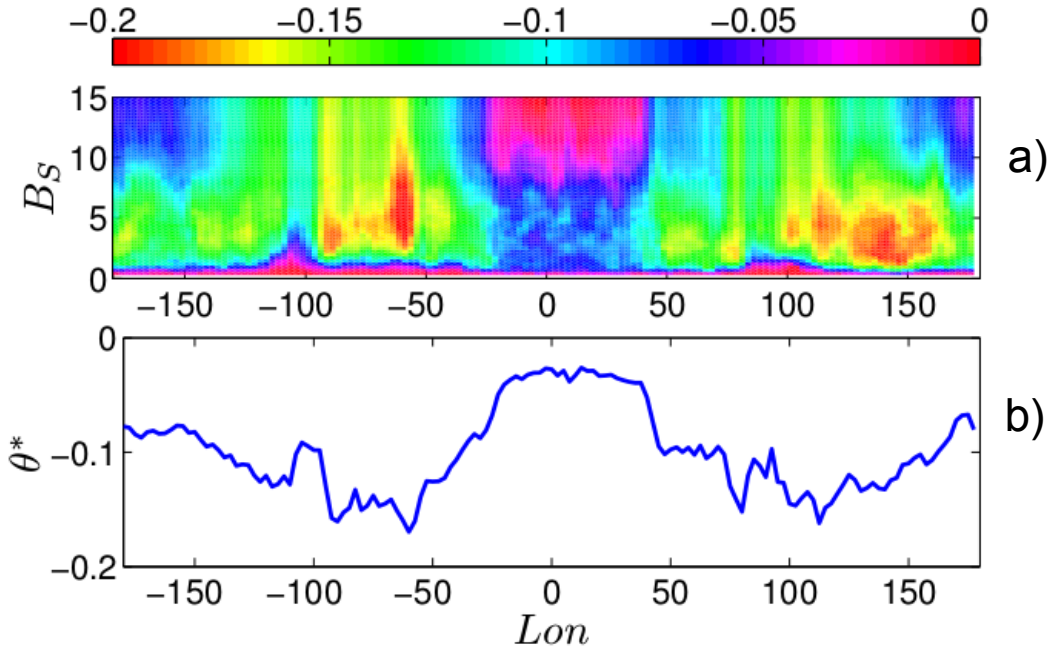

FIG. 4: a): Extremal indices θ^* (color scale) as a function of longitude and the Tibaldi-Molteni blocking index $B_S(t)$. b): extremal index averaged over all B_S vs longitude. Negative values indicate the presence of unstable fixed points.

does not appear to be a robust feature. Although this simple analysis shows that unstable fixed points may be present in the blocked circulation, it does not reveal whether they can be found for the zonal flow as well, contrary to our initial hypothesis. We will investigate in a further study whether such specificity is associated with a lack of predictability of the blocking dynamics for this region.

In order to have a detailed geographical description of the local clustering features, we will consider the local blocking index introduced by Pelly et al. in [23] and [34]. This blocking index B is a macroscopic measure of the strength of the meridional gradient of potential temperature on the isopotential vorticity surface with value 2 PVU (also called the PV2 surface; 1 PVU [1×10^{-6} K m^2 kg^{-1} s^{-1}]. This surface corresponds approximately to the tropopause, as described in [35]. B is computed every 5° of longitude as the difference of the average of potential temperature for regions 15° of latitude. Whenever B takes positive values, it is referred to as local instantaneous blocking. Negative values of B correspond instead to the westerlies mid-latitude circulation associated with the zonal flow. The more

negative B, the stronger such a circulation.

We computed θ^* at each grid point for 100 values of ζ, uniformly spaced between $\min(B)$ and $\max(B)$. We then averaged θ^* for two B intervals corresponding respectively to blocked regimes $B > 0$ and zonal flows $B < 0$, as shown in the left and right panels of Figure 5. Note also that only grid points with sufficient statistics to obtain reliable values of θ^* have been considered. We first investigate the difference between positive and negative B. For $B < 0$ (blocked flows), $\theta^* \neq 0$ appears almost everywhere. Strong geographical differences appear in the distribution of θ^*: negative θ^* are concentrated at higher latitudes, especially at polar latitudes over Canada where $\theta^* \simeq -0.15$. Interestingly, the dynamics over this region has been recognized also by [11] as a driver of the development of blocking structures. In the same paper, it has been argued that the precursor of transitions to the blocked circulation can be found by considering the weather evolution over this region. Other areas show instead positive values of θ^*. Such regions include the southern Mediterranean area, Japan and the mid-latitude Pacific Ocean. In these regions the tendency is rather to disrupt blocking structures.

We can compare the longitudinal averages of B reported in Figure 6 with the Tibaldi-Molteni index (Figure 4). We can also analyse the negative values of the Tibaldi-Molteni index B associated with the zonal circulation, which show no or weak clustering. B attains maxima around 50° W and 100° E. The magnitude is different due to the longitudinal averaging performed on B. Overall, the two blocking indices are consistent. This indicates that our results are robust. Moreover, as illustrated by the behavior of low-dimensional dynamical systems, the presence of unstable fixed points is associated with the blocked regime only. The dominant zonal regime seems to correspond to the generic points of a chaotic attractor, for which no special clustering structure occurs.

IV. ANALYSIS OF NAO AND AO ATMOSPHERIC INDICES

Although local indices provide comprehensive geographical information about the atmospheric circulation, one-dimensional indicators have been extensively used to characterize and forecast specific phenomena (see [36] and references therein).

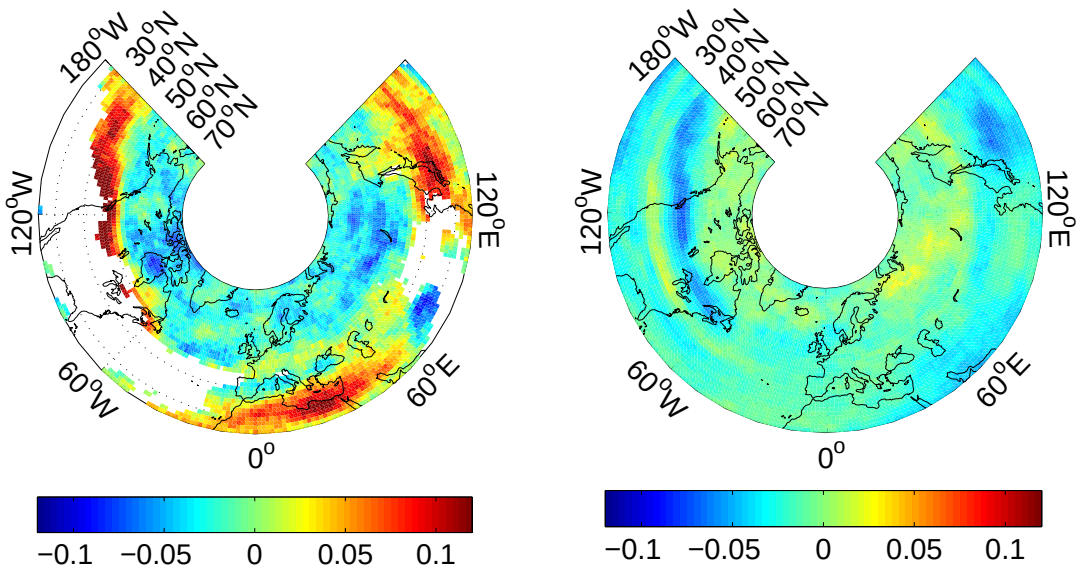

FIG. 5: Residual extremal index θ^* for two different ranges of the bidimensional blocking index B defined by Pelly et al. [23]. Left panel: θ^* averaged over $B > 0$ values corresponding to blocked flow regimes. Right panel: θ^* averaged over $B < 0$ values corresponding to the zonal flow regime. See text for descriptions.

Over Europe, the transition between zonal and blocked atmospheric dynamics has been historically associated to the so-called North Atlantic Oscillation (NAO) index, defined as the difference in pressure between Lisbon and Reykjavik [37]. The positive phase of the NAO reflects below-normal heights and pressure across the high latitudes of the North Atlantic and above-normal heights and pressure over the central North Atlantic, the eastern United States and western Europe. The negative phase reflects an opposite pattern of height and pressure anomalies over these regions [38].

The Arctic Oscillation index (AO) is more representative of the blocking dynamics over the entire northern hemisphere: it is constructed by projecting the daily (00Z) 1000mb height anomalies pole-ward of 20°N onto the leading mode of the Empirical Orthogonal Function (EOF) analysis of monthly mean 1000mb height during the years 1979-2000 [39]. Hence, the AO index behaves like a zonal average of the Tibaldi-Molteni index. In the negative

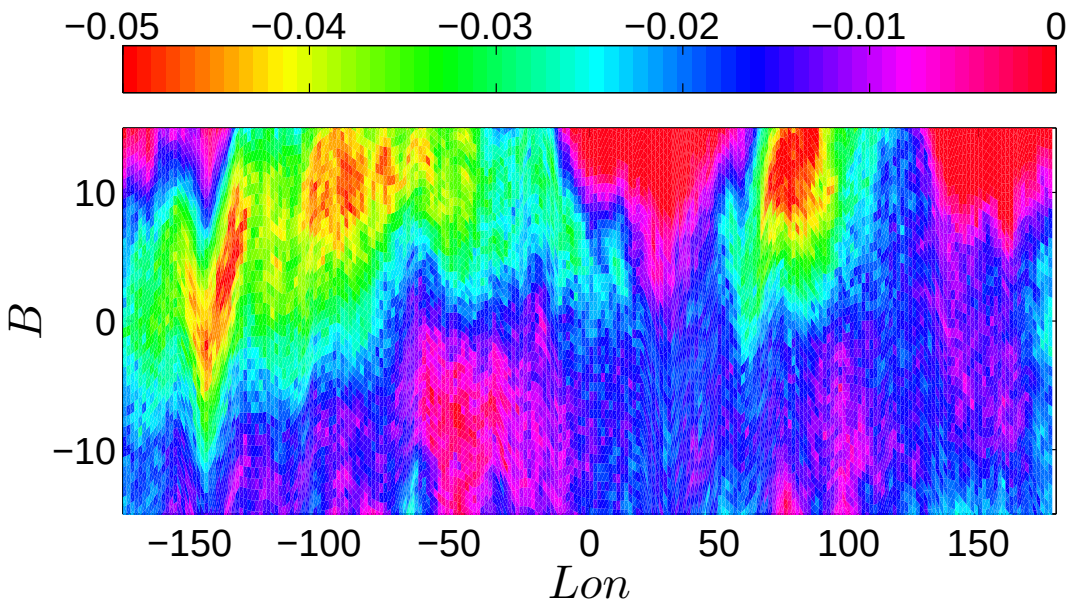

FIG. 6: Upper panel: Residual Extremal indices θ^* versus longitude for the blocking index B . Negative values indicate the presence of unstable fixed points.

phase, the polar low pressure system (also known as the polar vortex) over the Arctic is weaker, which results in weaker zonal flow. When the AO is positive the polar circulation is stronger and forces cold air and storms to remain farther north. The NAO and AO indices exhibit considerable inter-seasonal and inter-annual variability, and prolonged periods of both positive and negative phases of the pattern are not rare [39]. The daily NAO and AO data used in this paper are maintained by the US Climate Prediction Center [40].
With the analysis of a one-dimensional index, we can explore the link between complex atmospheric dynamics and simple one-dimensional observables. A priori, there is no reason why the two indices should provide the same information. The AO is a global average, the NAO a local observable. While they are both one-dimensional time series, we will keep in mind their substantially different origin.

We start by analysing the time series and the histograms shown in Fig. 7. The distributions of both NAO and AO are unimodal and peaked around zero, roughly similar to a Gaussian. the indices seem to spend most of their time around zero values with noisy fluctuations superimposed. A thirty-day moving average filter (green curves) reproduces a unimodal histogram, and there is no evidence that the time series oscillates between two states. It is

therefore hard to recognize in the data any trace of bistability or multistability.

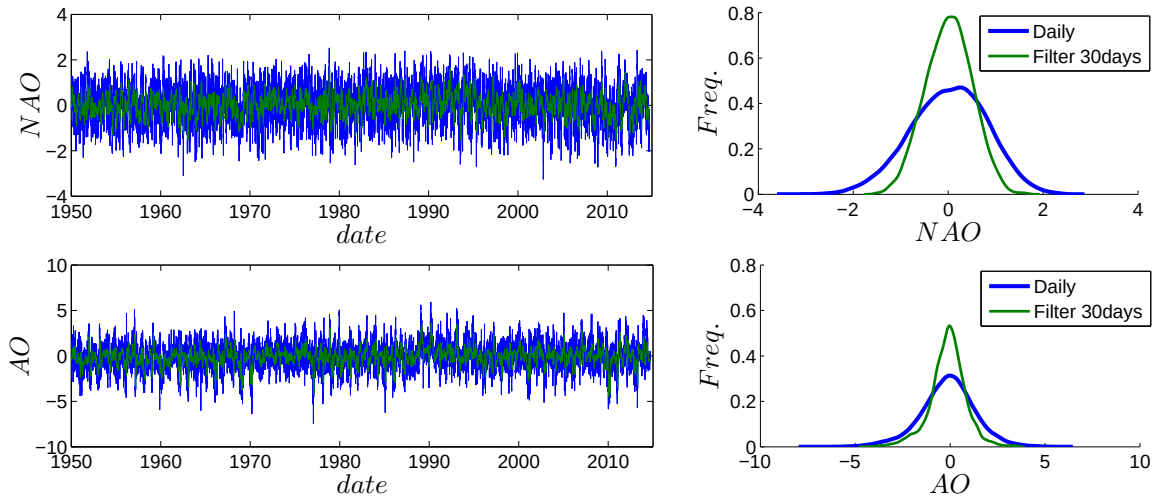

FIG. 7: NAO and AO daily time series (left panels) and their empirical density functions (right panels). Blue: original dataset, green: moving average filter over a 30 day window.

Even if we look at single episodes, a dynamical structure compatible with the existence of an unstable fixed point remains unclear: let us consider two *typical* examples of negative NAO and AO phases (upper and central panel of Fig. 8) and one positive phase (lower panels of Fig. 8) recorded respectively for September 2002, December 2010 and January 1988. As pointed out in the introduction, summer 2002 was characterised by a remarkable negative record of Arctic sea ice extent. For this event, the negative phases of NAO and AO seem to be comparable with the dynamics of the Hénon attractor around the fixed point ζ_u (Fig. 1b)), but the duration and intensity of the negative phases are different. In December 2010, Europe experienced a severe cold spell with extensive transport disruptions for several days. Although the NAO and the AO indices settle to negative values, the NAO oscillates over several values resembling that of a chaotic variable, whereas the AO seems to cluster for consecutive days around values of -4 and -2. For January 1988, the behavior of the indices look much more chaotic with oscillations associated with the mean lifetime of baroclinic structures (a few days). This latter regime can be compared to Fig.1c), i.e. with a typical point of the Hénon attractor. The contradicting results obtained for single episodes imply that the existence of an unstable fixed point must be assessed statistically

via the computation of θ^*.

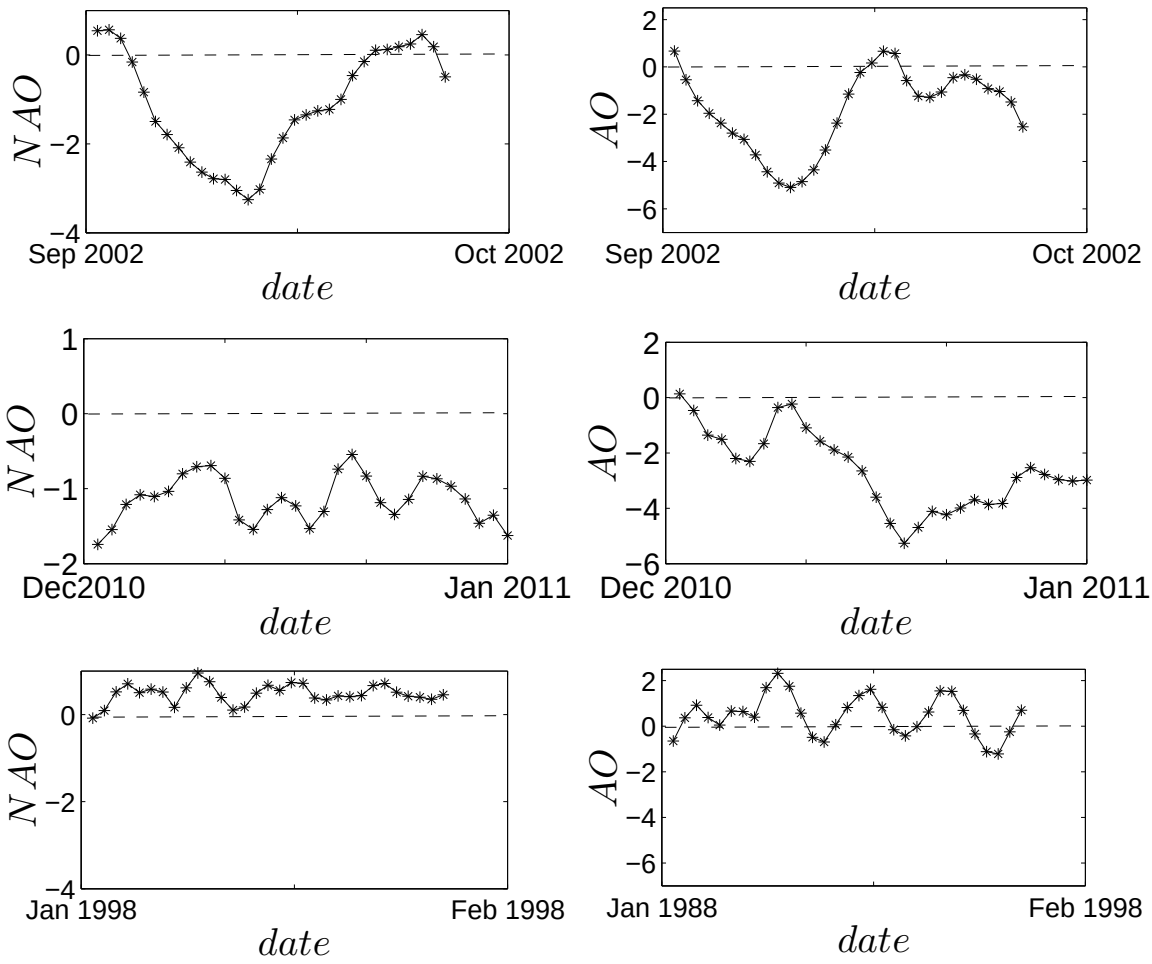

FIG. 8: NAO (left) and AO (right) daily time series for some specific events. Upper panels: September 2002. Central panels: December 2010. Lower panels: January 1988

After applying the procedure described in Section 2-B, we obtain, for each value of the NAO and AO, the residual extreme value index θ^*, as shown in Fig. 9. We recall that for NAO and AO values around zero there is no additional clustering, i.e. no unstable fixed points can be detected. The behavior of the two indices is indeed different. θ^* is negative for negative AO, following the core hypothesis of this paper that blocked circulation can be associated with the existence of unstable fixed points. In contrast, θ^* is positive for positive NAO.

There is no reason why the two indices should follow the same behavior. Features of the

NAO are compatible with that observed for the Tibaldi-Molteni and the Pelly index around 0° longitude, where the blocked flow was not associated with negative θ^*. The disruption of clusters for positive NAO corresponding to zonal flow is compatible with the presence of complex geography, which tends to destroy the typical time scales of baroclinic instability (1.5 to 3 days). It is encouraging that one can find the trace of the existence of unstable fixed points for the AO index, i.e., that the global average does not erase the clustering properties found for B and B_S. This analysis indeed suggests that the AO is more sensitive to blocking phenomena than the NAO. We thus can account for the empirical observation of [41].

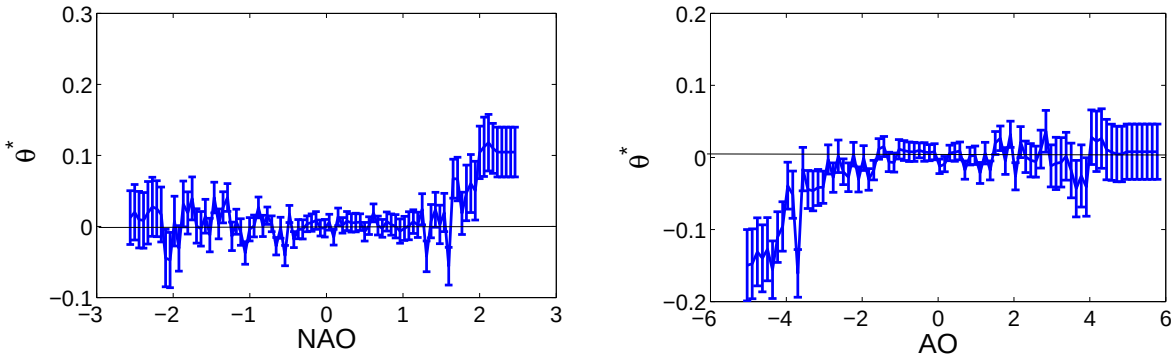

FIG. 9: Residual extremal index θ^* for the NAO index (left) and the AO index (right). Error bars represent a standard deviation of the mean taken over the ensemble of 100 surrogates.

V. CONCLUSION AND DISCUSSION

In this paper, we have adapted the concept of the extremal index, as applied in dynamical systems, to the analysis of atmospheric indices which describe the switching between zonal flow to blocked flow in the atmospheric mid-latitude circulation. We have presented evidence that the switching between atmospheric and blocked circulation can be associated with the existence of an unstable (saddle) fixed point of the atmospheric dynamics. The novelty of this approach lies in the use of observations, rather than intermediate complexity models or GCM. Our results appear to be robust across blocking indices, and are consistent with mid-latitude circulation mechanisms and local geography.

Another remarkable result is that such information is preserved in the AO time series, which is a global average of the Tibaldi-Molteni index. On the other hand, it warns against the use of local indices, such as the NAO time series, outside areas where they have been defined.

This paper has illustrated a novel approach to statistical and dynamical modeling: in [12] the properties of blocking indices have been widely investigated and compared to the statistics of stationary red noise process. The authors argued that the statistical model was not sufficient to describe the characteristics of blocking and claimed that the persistence beyond that given by a red noise model is due to the self-sustaining nature of the blocking phenomenon. Here, we have shed light on this self-sustaining nature: When the circulation settles in a blocked regime, the presence of unstable fixed points gives rise to the persistence (the self-sustaining nature) of quasi-stationary conditions. In order to improve the statistical modeling of blocking phenomena, one has to account for local clustering effects in statistical models, which is a non-trivial challenge.

VI. ACKNOWLEDGEMENTS

DF and PY were supported by the ERC Grant A2C2 (No. 338965).

[1] J. R. Holton and G. J. Hakim, *An introduction to dynamic meteorology* (Academic press, 2013).

[2] J. G. Charney, Journal of Meteorology **4**, 136 (1947).

[3] K. Emanuel, Nature **436**, 686 (2005).

[4] I. Rudeva, Izvestiya, Atmospheric and Oceanic Physics **44**, 273 (2008).

[5] P. Yiou, R. Vautard, P. Naveau, and C. Cassou, Geophysical Research Letters **34** (2007).

[6] M. Serreze, J. Maslanik, T. Scambos, F. Fetterer, J. Stroeve, K. Knowles, C. Fowler, S. Drobot, R. Barry, and T. Haran, Geophysical Research Letters **30** (2003).

[7] B. Legras and M. Ghil, Journal of the atmospheric sciences **42**, 433 (1985).

[8] M. Ghil, in *Irreversible Phenomena and Dynamical Systems Analysis in Geosciences* (Springer, 1987), pp. 241–283.

[9] K. Mo and M. Ghil, Journal of Geophysical Research: Atmospheres (1984–2012) **93**, 10927 (1988).

[10] E. R. Weeks, J. C. Crocker, A. C. Levitt, A. Schofield, and D. A. Weitz, Science **287**, 627 (2000).

[11] R. Vautard, Monthly Weather Review **118**, 2056 (1990).

[12] G. Masato, B. J. Hoskins, and T. J. Woollings, Journal of the Atmospheric Sciences **66**, 2143 (2009).

[13] G. Masato, B. Hoskins, and T. J. Woollings, Quarterly Journal of the Royal Meteorological Society **138**, 1285 (2012).

[14] R. Benzi, G. Paladin, G. Parisi, and A. Vulpiani, Journal of Physics A: Mathematical and General **18**, 2157 (1985).

[15] L. E. Payne and D. Sattinger, Israel Journal of Mathematics **22**, 273 (1975).

[16] J. L. Kaplan and J. A. Yorke, in *Functional Differential equations and approximation of fixed points* (Springer, 1979), pp. 204–227.

[17] A. C. M. Freitas, J. M. Freitas, and M. Todd, Probability Theory and Related Fields **147**, 675 (2010).

[18] V. Lucarini, D. Faranda, G. Turchetti, and S. Vaienti, Chaos: An Interdisciplinary Journal of Nonlinear Science **22**, 023135 (2012).

[19] A. C. M. Freitas, J. M. Freitas, and M. Todd, Advances in Mathematics **231**, 2626 (2012).

[20] D. Faranda, J. M. Freitas, V. Lucarini, G. Turchetti, and S. Vaienti, Nonlinearity **26**, 2597 (2013).

[21] D. Faranda and S. Vaienti, Geophysical Research Letters **40**, 5782 (2013).

[22] S. Tibaldi and F. Molteni, Tellus A **42**, 343 (1990).

[23] J. L. Pelly and B. J. Hoskins, Journal of the atmospheric sciences **60**, 743 (2003).

[24] V. Lucarini, R. Blender, C. Herbert, S. Pascale, and J. Wouters, arXiv preprint arXiv:1311.1190 (2013).

[25] A. Katok and B. Hasselblatt, *Introduction to the modern theory of dynamical systems*, vol. 54 (Cambridge university press, 1997).

[26] M. Hénon, Communications in Mathematical Physics **50**, 69 (1976).

[27] M. Süveges, Extremes **10**, 41 (2007).

[28] D. Faranda, V. Lucarini, G. Turchetti, and S. Vaienti, Journal of Statistical Physics **145**, 1156

(2011).

[29] P. J. Brockwell and R. A. Davis, *Introduction to time series and forecasting*, vol. 1 (Taylor & Francis, 2002).

[30] T. Schreiber and A. Schmitz, Physical Review Letters **77**, 635 (1996).

[31] S. C. Scherrer, M. Croci-Maspoli, C. Schwierz, and C. Appenzeller, International journal of climatology **26**, 233 (2006).

[32] S. Tibaldi, E. Tosi, A. Navarra, and L. Pedulli, Monthly Weather Review **122**, 1971 (1994).

[33] F. d'Andrea, S. Tibaldi, M. Blackburn, G. Boer, M. Déqué, M. Dix, B. Dugas, L. Ferranti, T. Iwasaki, A. Kitoh, et al., Climate Dynamics **14**, 385 (1998).

[34] E. Tyrlis and B. Hoskins, Journal of the Atmospheric Sciences **65**, 1638 (2008).

[35] B. J. Hoskins, I. N. James, and G. H. White, Journal of the atmospheric sciences **40**, 1595 (1983).

[36] J. W. Hurrell and C. Deser, Journal of Marine Systems **79**, 231 (2010).

[37] J. W. Hurrell, Science **269**, 676 (1995).

[38] J. W. Hurrell, Y. Kushnir, G. Ottersen, and M. Visbeck, *An overview of the North Atlantic oscillation* (Wiley Online Library, 2003).

[39] D. W. Thompson and J. M. Wallace, Geophysical Research Letters **25**, 1297 (1998).

[40] NOAA, *North atlantic oscillation* (2015), URL `http://www.cpc.ncep.noaa.gov/data/teledoc/nao.shtml`.

[41] M. H. Ambaum, B. J. Hoskins, and D. B. Stephenson, Journal of Climate **14**, 3495 (2001).